RSC Advances

ROYAL SOCIETY OF CHEMISTRY

www.rsc.org/advances

Table of Contents entry

Sun-light-driven Photocatalytic Activity by ZnO/Ag Heteronanostructures Synthesized via Facile Thermal Decomposition Approach

Syam Kandula and Pethaiyan Jeevanandam*

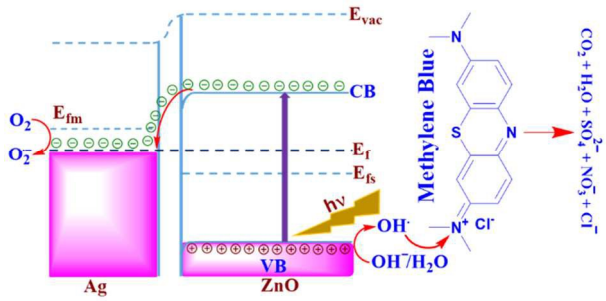

ZnO/Ag heteronanostructures with good photocatalytic activity towards photodegradation of methylene blue have been synthesized using a facile thermal decomposition approach.

RSC Advances

ARTICLE

Sun-light-driven Photocatalytic Activity by ZnO/Ag Heteronanostructures Synthesized via Facile Thermal Decomposition Approach

Received 00th January 20xx,
Accepted 00th January 20xx

DOI: 10.1039/x0xx00000x

www.rsc.org/

Syam Kandula and Pethaiyan Jeevanandam*

ZnO/Ag heteronanostructures with varying amounts of silver nanoparticles on ZnO nanorods were successfully synthesized via a novel and economical thermal decomposition approach. ZnO nanorods were first synthesized by homogeneous precipitation method and silver nanoparticles were subsequently deposited on the surface of ZnO nanorods by the thermal decomposition of silver acetate in diphenyl ether at 220 ^{o}C. The amount of silver nanoparticles on the ZnO nanorods was controlled by varying the concentration of silver acetate during the thermal decomposition. The synthesized ZnO/Ag heteronanostructures were characterized by X-ray diffraction (XRD), field emission scanning electron microscopy (FE-SEM), energy dispersive X-ray analysis (EDXA), transmission electron microscopy (TEM), X-ray photoelectron spectroscopy (XPS), UV-Visible diffuse reflectance spectroscopy (DRS), and photoluminescence (PL) spectroscopy. XRD results confirm the presence of silver nanoparticles (size = 24-31 nm) in the ZnO/Ag heteronanostructures. SEM and TEM images prove the presence of silver nanoparticles on the surface of ZnO nanorods. XPS results indicate the presence of metalic silver in ZnO/Ag. DRS results show characteristic surface plasmon resonance absorption due to silver nanoparticles and PL results indicate an effective separation of photogenerated electron–hole pairs in the ZnO/Ag heteronanostructures as compared to pristine ZnO nanorods. The synthesized ZnO/Ag heteronanostructures were explored as catalyst towards the photodegradation of methylene blue in an aqueous solution and photostability of the ZnO/Ag heteronanostructures has also been demonstrated.

1. Introduction

Semiconductors (e.g. ZnO, TiO_2, SnO_2, CdS, etc.) have been explored as effective photocatalysts and their band structure possess a filled valence band (VB) and an empty conduction band (CB).[1–4] Photocatalytic degradation of organic compounds involves the following steps: (i) when the energy of a photon is higher than or equal to the band gap of the semiconductor, electrons are excited from the VB to the CB with the creation of equal number of holes in the VB; (ii) the photogenerated excitons (electron-hole pairs) are trapped by dissolved oxygen in the aqueous solution resulting in the production of reactive oxidizing species (ROS), for example, $^{\bullet}$OH; and (iii) the ROS attack and mineralize the adsorbed organic molecules. In a semiconductor, the photogenerated excitons easily undergo recombination which decreases the photocatalytic activity.[2,3,5] To overcome this limitation, semiconductor based nanomaterials such as core-shell/ yolk-shell nanoparticles, nanorattles, and nanocomposites have been developed and these nanomaterials exhibit better and tunable physicochemical properties.[6–9] Researchers have made effort to develop metal-semiconductor and semiconductor-semiconductor nanocomposites and have used them in various applications such as catalysis, sensors, and optoelectronics.[10–13] Metal-semiconductor composite heteronanostructures have been extensively used as photocatalysts and these composites enhance the photocatalytic efficiency by reducing the electron-hole pair recombination. The photogenerated electrons in the conduction band of the semiconductor transfer to the metal which enables lower recombination rate of the photogenerated excitons, with the photogenerated holes remaining in the valence band of the semiconductor. The metal acts as an electron sink due to the Schottky barrier at the metal-semiconductor interface.[14–16]

Among the metal oxide semiconductors, ZnO is a good photocatalyst due to its wide band gap (3.38 eV), high exciton binding energy (60 meV), low cost, and its non-toxic nature.[17] ZnO exhibits good photocatalytic activity for the photodegradation of different organic dyes.[18–20] As compared to zero dimensional (0-D) ZnO nanoparticles, one dimensional (1-D) nanorods exhibit higher catalytic activity due to fast electron transfer.[21] However, the fast electron-hole recombination in ZnO reduces its photocatalytic efficiency. To overcome this limitation, metal (e.g. silver, gold, and platinum) deposited semiconductor (ZnO) nanocomposite materials have

Department of Chemistry,
Indian Institute of Technology Roorkee,
Roorkee–247667, India
**E-mail: jeevafcy@iitr.ac.in*
Tel: +91–1332–285444; Fax: 91–1332 –273560.

been produced.[22–24] The formation of Schottky barrier at the metal-semiconductor interface reduces the electron-hole pair recombination. Among the noble metals, silver is the most sought after metal due to its good chemical stability, low-cost and high efficiency.[25,26] Moreover, the surface plasmon resonance absorption of silver nanoparticles creates a local electric field which enhances the photocatalytic activity.

Different chemical and physical methods have been reported for the synthesis of ZnO/Ag heteronanostructures. The chemical methods include electrodeposition, hydrothermal/ solvothermal, micro-emulsion, seed mediated growth, sol-gel, wet chemical, sonochemical, thermal decomposition, and photocatalytic reduction.[27–36] The physical methods include electron beam evaporation, laser assisted fabrication, and microwave assisted route.[37–40] The synthesized ZnO/Ag heteronanostructures have been used in different applications such as surface enhanced Raman scattering, photodegradation of toxic organic dyes, photoelectrochemical cells, bactericides, sensors, and field emission.[41–43] Lu et al., Zheng et al., Wu et al., and Shan et al. have synthesized ZnO/Ag heteronanostructures by hydrothermal method and have used them as photocatalyst for the degradation of orange-II, methyl orange, rhodamine B, and rhodamine 6G, respectively.[28,29,44,45] Ren et al., Chen et al., and Lin et al. have prepared the ZnO/Ag heteronanostructures via photochemical deposition and have used them as photocatalyst for the degradation of methylene blue, methyl orange, and rhodamine 6G, respectively.[35,39,46] Sun et al. have prepared the ZnO/Ag heteronanostructures using chemical reduction and have used them as photocatalyst for the degradation of methylene blue.[47]

The preparation of ZnO/Ag heteronanostructures with uniformly deposited silver nanoparticles on ZnO nanorods without free silver particles is still a challenge due to self-nucleation of silver nanoparticles during the deposition of silver on ZnO. In the present study, a facile, economical, and simple thermal decomposition approach for the synthesis of ZnO/Ag heteronanostructures has been reported. The particle size of silver nanoparticles on the ZnO nanorods could be controlled simply by varying the concentration of silver acetate during the thermal decomposition. The synthesized ZnO/Ag heteronanostructures were characterized by various techniques and they were explored as photocatalyst for the degradation of methylene blue in an aqueous solution under sunlight irradiation.

2. Experimental

2.1. Reagents

Zinc nitrate (99%, SRL, AR), urea (99.5%, Rankem, AR), ethylene glycol (99%, Rankem, LR), silver acetate (98%, Loba Chemie), diphenyl ether (99%, Sigma-Aldrich), and methylene blue (SRL) were used as received without further purification. Methanol was received from SD Fine Chemicals and was used after distillation. More details on the synthetic procedure for the preparation of ZnO/Ag heteronanostructures are discussed below.

2.2. Synthesis

2.2.1. Synthesis of ZnO nanorods

ZnO nanorods were synthesized using homogeneous precipitation method. [48,49] In a typical synthesis, 100 mL of 0.05 M zinc nitrate solution (solvent = mixture of ethylene glycol and water (1:1 vol %)) and 100 mL of 0.25 M urea solution were mixed in a beaker and stirred at 90 ^{o}C for 6 h. The contents were allowed to cool to room temperature, filtered, washed with water and dried in an oven for overnight at 70 ^{o}C.

2.2.2. Synthesis of ZnO/Ag heteronanostructures

About 50 mg of ZnO nanorods was mixed with different amounts of silver acetate (0.10, 0.15 and 0.25 mmol) in 10 mL of diphenyl ether and the contents were sonicated for about 3 minutes to achieve good dispersion. The contents were refluxed at about 220 ^{o}C for 1 h in air. After completion of the reaction, the obtained slurry was cooled to room temperature and then 25 mL of methanol was added. The obtained precipitate was centrifuged, washed with methanol several times and dried in an oven for overnight. The obtained silver deposited ZnO samples were labelled as A1, A2, and A3 corresponding to 0.10, 0.15, and 0.25 mmol concentration of silver acetate, respectively.

2.3 Characterization

X-ray diffraction patterns of the samples were recorded in the 2θ range 25-90^{o} on a Brucker AXS D8 diffractometer and the scan speed was 2 ^{o}/min. Copper was used as the target (Cu-K_{α}; λ = 1.5406 Å). The surface morphological studies and energy dispersive X-ray analysis were carried out using a Carl Zeiss ULTRA plus field emission scanning electron microscope operating at 15 kV. TEM images of the samples were recorded by employing a FEI TECNAI G^2 20S-TWIN microscope operating at 200 kV. The surface composition of the ZnO/Ag sample was analyzed on a VG microtech ESCA (XPS) 3000 spectrometer using Al K_{α} X-ray source. The band gap (E_g) measurements were carried out on a Shimadzu UV-2450 UV-Visible spectrometer attached with a diffuse reflectance accessory in the wavelength range 200-800 nm and $BaSO_4$ was used as the reference. Photoluminescence (PL) measurements were carried out using a Shimadzu RF 5301-PC photoluminescence spectrometer. For the PL measurements, 5 mg of the each powder sample was dispersed in about 5 mL of methanol and sonicated for a few minutes. The excitation wavelength used was 325 nm and both the excitation and emission slit widths were 5 nm.

2.4. Photocatalytic experiments

The photocatalytic activity of the synthesized ZnO/Ag heteronanostructures was tested under sunlight irradiation and methylene blue was chosen as the model dye. All the photocatalytic experiments were carried out at Indian Institute of Technology Roorkee between 11:30 am to 13:00 pm in the month of May 2015. The average sunlight intensity at Roorkee (the latitude and longitude are 29^{o}52′ N and 77^{o}53′ E,

respectively) in the month of May 2015 was 245 Watt/m^2.[50] In a typical photocatalytic experiment, about 25 mg of the photocatalyst (ZnO/Ag heteronanostructures (A1, A2 and A3), ZnO nanorods or silver nanoparticles) was dispersed in 100 mL of 1×10^{-5} M methylene blue aqueous solution in a beaker and stirred in dark for about 20 minutes to achieve adsorption-desorption equilibrium. After this, the beaker was kept under the exposure of sunlight for about 90 minutes. During the photocatalytic experiments, about 5 mL each aliquots were withdrawn at regular time intervals, centrifuged and the supernatant solutions were analyzed using UV-Visible spectroscopy. A blank reaction was also carried out without using any catalyst under similar experimental conditions. The percent degradation of methylene blue was estimated using the following formula,

$$\% \text{ Degradation} = (1\text{-}C/C_o) \times 100$$

where C_o and C are the concentrations of methylene blue at adsorption equilibrium and at irradiation time 't', respectively.

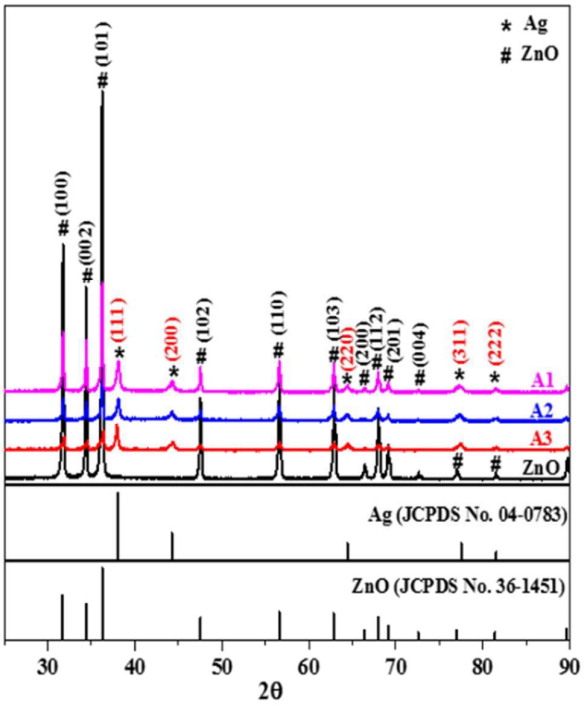

Fig. 1 XRD patterns of ZnO and ZnO/Ag heteronanostructures (A1, A2 and A3).

3. Results and discussion

The XRD patterns of pure ZnO and ZnO/Ag heteronanostructures (A1, A2 and A3) are shown in Figure 1. Pure ZnO shows diffraction peaks at 2θ values of 31.61°, 34.41°, 36.24°, 47.61°, 56.59°, 62.87°, 66.31°, 67.94°, 69.06°, 72.54°, 76.96°, and 81.31° attributed to (100), (002), (101), (102), (110), (103), (200), (112), (201), (004), (202), and (104) planes of wurzite ZnO (JCPDS file no. 36-1451), respectively. All the as prepared ZnO/Ag samples show two set of diffraction peaks. The diffraction peaks marked with "#" indicate peaks due to wurzite ZnO. The peaks marked with "*" at 2θ values of 38.12°, 44.32°, 64.46°, 77.47°, and 81.53° correspond to (111), (200), (220), (311), and (222) planes of face centered cubic silver (JCPDS file no. 04-0783), respectively. The crystallite size of ZnO and silver in all the ZnO/Ag samples was calculated using Debye-Scherrer formula using the XRD peaks at 2θ = 36.24° and 38.12°, respectively. The crystallite size of pure ZnO is about 50 nm. In the ZnO/Ag samples, the crystallite size of silver nanoparticles was found to be 24 nm, 26 nm, and 31 nm and the crystallite size of ZnO was 48 nm, 42 nm and 35 nm for the samples A1, A2, and A3, respectively. In the ZnO/Ag samples, the decrease in the crystallite size of the ZnO compared to pure ZnO is attributed to the deposition of silver nanoparticles on its surface.

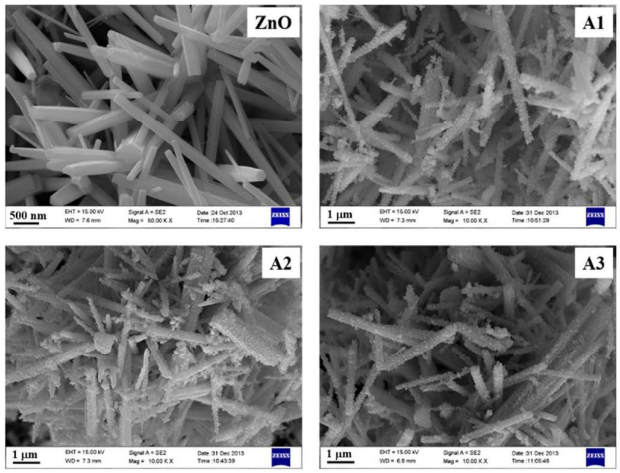

Fig. 2 FE-SEM images of ZnO nanorods and ZnO/Ag heteronanostructures (A1, A2 and A3).

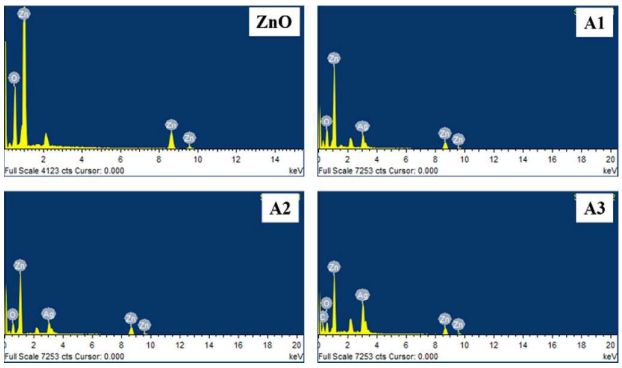

Fig. 3 EDX spectra of ZnO nanorods and ZnO/Ag heteronanostructures (A1, A2 and A3).

The morphological studies were first carried out using FE-SEM analysis and the FE-SEM images of pure ZnO nanorods and the ZnO/Ag heteronanostructures (A1, A2, and A3) are shown in Figure 2. The length and diameter of pure ZnO nanorods were found to be about 2.5 ± 0.4 μm and 260 ± 20 nm, respectively. The FE-SEM images of ZnO/Ag samples (A1 to

A3) show clearly the deposition of silver on the ZnO nanorods. The particle size values of silver in the ZnO/Ag heteronanostructures are 53.5 ± 15.7 nm, 62.3 ± 14.2 nm, and 70.2 ± 16.4 nm for samples A1, A2, and A3, respectively. As the concentration of silver increases from sample A1 to A3, the particle size of silver also increases. Furthermore, the elemental composition of ZnO/Ag heteronanostructures was estimated using energy dispersive X-ray analysis and the results are shown in Figure 3. The EDXA results of ZnO/Ag heteronanostructures show the presence of zinc, oxygen, and silver in all the samples (A1, A2 and A3). The weight percent of silver in the ZnO/Ag heteronanostructures was found to be 20.4 ± 2.3, 25.4 ± 1.9, and 26.6 ± 3.7 for the samples A1, A2 and A3, respectively.

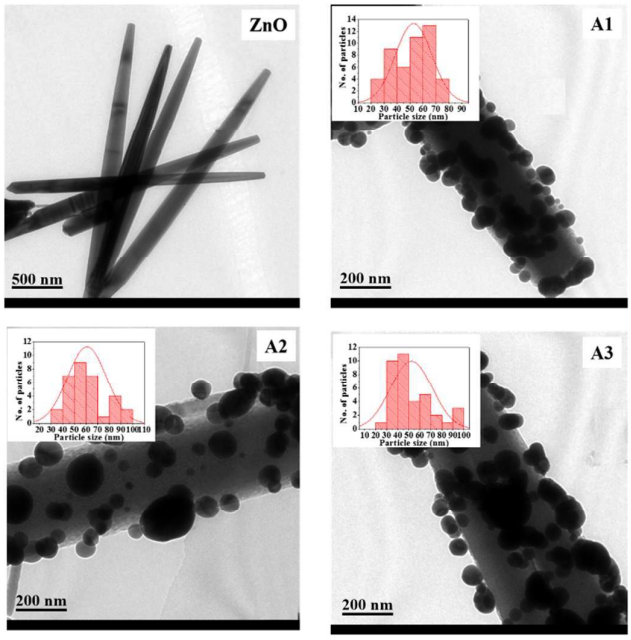

Fig. 4 TEM images of ZnO and ZnO/Ag heteronanostructures (A1, A2 and A3).

To understand the ZnO/Ag heteronanostructures better, TEM analysis was carried out for pure ZnO and ZnO/Ag heteronanostructures and the TEM images are shown in Figure 4. The length of pure ZnO nanorods is about 2.5 ± 0.15 µm and the diameter is about 200 ± 20 nm. In the TEM images of the ZnO/Ag heteronanostructures (A1, A2 and A3), one can clearly see adhered silver nanoparticles on the surface of ZnO nanorods; no free silver nanoparticles are found in the TEM images. The particle size distribution of silver nanoparticles on the ZnO nanorods are shown as insets in the corresponding TEM images. The mean diameter of silver nanoparticles on ZnO nanorods was found to be 52.8 ± 14.1 nm, 60.7 ± 16.7 nm, and 68.4 ± 8.8 nm for samples A1, A2, and A3, respectively. The broad size distribution of silver nanoparticles on ZnO nanorods is attributed to site-selective positioning of silver on ZnO nanorods prompted via a small lattice mismatch between silver and ZnO at the respective crystallographic plane.[40] The nucleation of silver takes place on energetically favored (101) plane of ZnO nanorods and then the silver clusters are formed at different positions on the ZnO nanorods. The SAED patterns of pure ZnO and ZnO/Ag samples are shown in Figure 5. Pure ZnO nanorods showed a set of diffraction spots in the SAED patterns due to hexagonal wurzite structure which indicates single crystalline nature of the ZnO nanorods. The distance between the two consecutive spots in the SAED pattern of pure ZnO was found to be 0.263 nm which is attributed to (002) plane of hexagonal ZnO which suggests the preferential growth of ZnO nanorods along (001) direction.[51] The SAED patterns of ZnO/Ag heteronanostructures show spot patterns due to ZnO and ring patterns due to cubic silver.

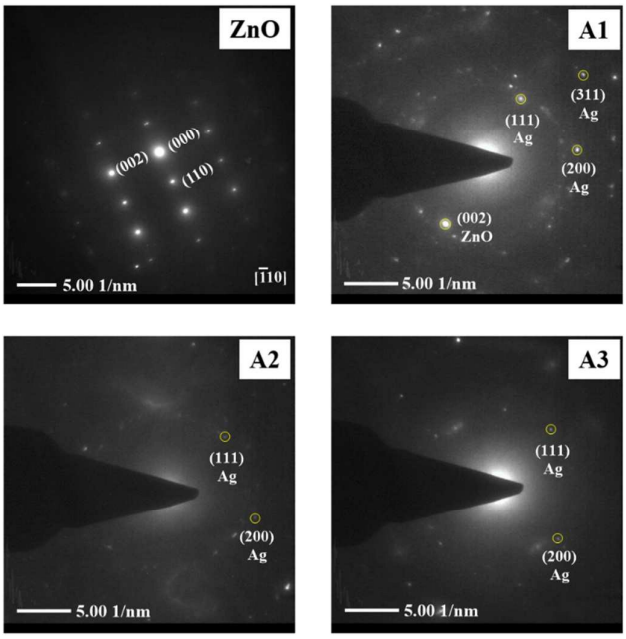

Fig. 5 SAED patterns of ZnO and ZnO/Ag heteronanostructures (A1, A2 and A3).

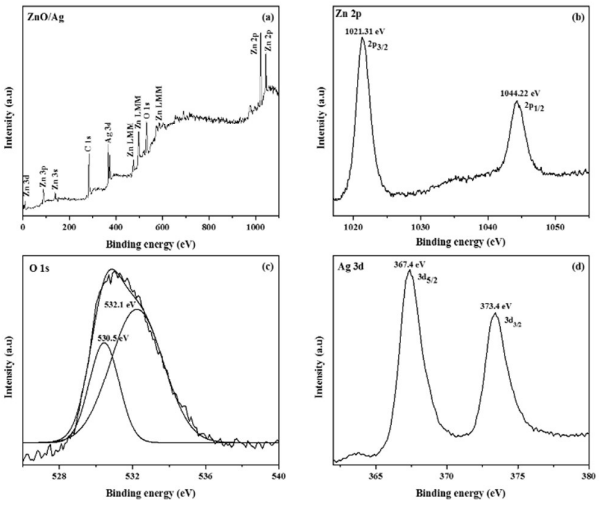

Fig. 6 (a) XPS survey spectra of ZnO/Ag sample A1, and (b-d) high resolution XPS spectra of Zn 2p, O 1s, and Ag 3d, respectively.

In order to understand if silver deposition on ZnO surface is in metallic form or not and also the surface composition of the ZnO/Ag sample, XPS analysis was carried out and the results are shown in Figure 6. The XPS results for ZnO/Ag (A1) indicate the presence of Zn, O, and Ag. The Zn $2p_{3/2}$ spectrum (Figure 6b) shows a peak centered at about 1021.3 eV. This is attributed to the presence of Zn^{2+} on the sample surface.[29] The O1s spectrum (Figure 6c) is asymmetric and the spectrum was deconvoluted. The deconvolution results suggest that there are two kind of oxygen species; the peak with binding energy of about 530.5 eV is due to lattice oxygen of ZnO and the XPS peak at about 532.1 eV is due to the oxygen of surface hydroxyls.[28] The Ag 3d spectrum (Figure 6d) shows two peaks with binding energies 367.4 eV (Ag $3d_{5/2}$) and 373.4 eV (Ag $3d_{3/2}$) with a splitting of 6 eV. The observed binding energies

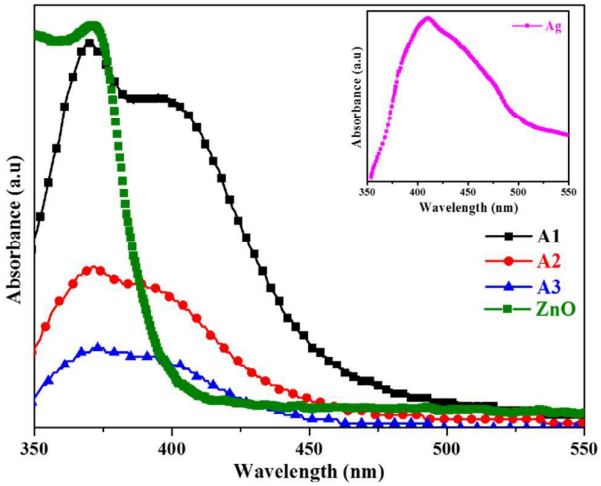

and the doublet splitting indicate the presence of metallic silver in the ZnO/Ag sample.[39] The ratio of Zn to Ag in ZnO/Ag sample (A1) was found to be 2.46.

Fig. 7 UV-Visible diffuse reflectance spectra of ZnO nanorods and ZnO/Ag heteronanostructures. The UV-Vis spectrum of Ag nanoparticles is shown as inset.

The optical properties of pure ZnO nanorods and ZnO/Ag heteronanostructures (A1, A2, and A3) were investigated using UV-Visible diffuse reflectance spectroscopy (DRS) and photoluminescence (PL) spectroscopy. The DRS spectra of pristine ZnO nanorods, and ZnO/Ag heteronanostructures are shown in Figure 7. The bulk band gap of pure ZnO is 3.38 eV[17] and pristine ZnO nanorods possess band gap absorption at 373 nm (3.33 eV). Quantum confinement effect is not observed in the case of ZnO nanorods due to their large diameter (about 250 nm) which is much higher than the Bohr exciton radius of ZnO (a_B = 1.8 nm). Pure Ag nanoparticles show surface plasmon resonance absorption at about 405 nm (inset in Figure 7). The DRS spectra of ZnO/Ag heteronanostructures show two prominent absorption bands in the UV-Visible region. The band at 370 nm is due to the band gap absorption of ZnO and the band at about 400 nm is due to the surface plasmon resonance of silver nanoparticles present in the ZnO/Ag heteronanostructures.

The room temperature photoluminescence (PL) spectra of pristine ZnO nanorods, pure Ag nanoparticles, and ZnO/Ag heteronanostructures (A1, A2 and A3) are shown in Figure 8. The PL spectrum of pristine ZnO nanorods show emission bands at 380 nm, 412 nm, 435 nm, 466 nm, 485 nm and 494 nm. The emission bands at 380 nm and 412 nm are attributed to band edge free exciton recombination of ZnO.[40,43] The multiple peaks in this region are due to the formation of different shallow levels inside the band gap due to the presence of interstitial zinc atoms.[40,52] The strong emission in the blue region at about 435 nm is attributed to the electronic transition between the excitonic level and the interstitial oxygen (O_i). The emission in the blue-green region (at 466 nm) is attributed to the electronic transition between a deep acceptor (V_{Zn}) and a shallow donor (Zn_i). The emission bands in the green region (at 485 nm 494 nm) are attributed to zinc vacancies, interstitial zinc and structural defects.[48] Pure Ag nanoparticles show a strong emission band at 357 nm and a broad emission between 400 and 600 nm. The strong emission band at 357 nm is attributed to radiative recombination of occupied electrons from the *sp* band with holes in the valence

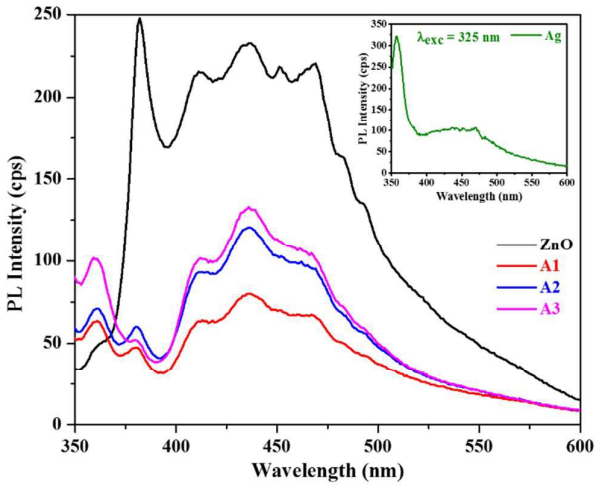

d band.[53] The broad emission between 400 and 600 nm is due to radiative decay of the surface plasmon resonance (SPR) excitation in the Ag nanoparticles.[54]

Fig. 8 Photoluminescence (PL) spectra of ZnO nanorods and ZnO/Ag heteronanostructures. The PL spectrum of Ag nanoparticles is shown as inset.

The PL spectra of ZnO/Ag heteronanostructures exhibit similar emission bands as that of pure ZnO nanorods and pure Ag nanoparticles with noticeable intensity reduction. The reduction in intensity observed in the PL spectra of ZnO/Ag heteronanostructures as compared to pure ZnO nanorods is attributed to an efficient interfacial charge transfer from the

ZnO nanorods to the silver nanoparticles; silver acts as an electron sink which traps the electrons from ZnO and hinder the recombination of photogenerated excitons in ZnO.[31] In the case of ZnO/Ag heteronanostructures, sample A1 exhibits lower PL emission intensity compared to the other ZnO/Ag samples and the PL intensity order is A1 < A2 < A3. The recombination of electron-hole pairs depends on the amount of silver nanoparticles present on the surface of ZnO nanorods. From A1 to A3, the amount of silver nanoparticles on the surface of ZnO nanorods increases and the extent of recombination of electron-hole pairs increases and accordingly, the PL intensity also increases in the same order. When sufficient amount of silver metal sites are present on the surface of ZnO nanorods (e.g. sample A1), these metal sites trap the electrons effectively and this leads to increase in the charge separation of photogenerated electron and hole pairs on the surface of ZnO nanorods.[44]

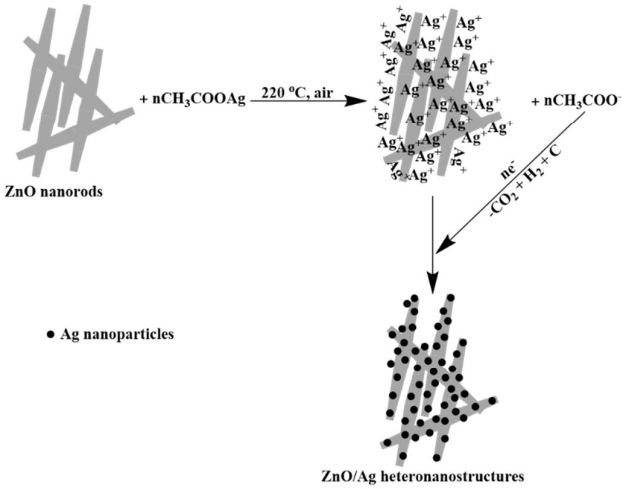

3.1. Mechanism of formation of ZnO/Ag heteronanostructures

Scheme 1. The proposed mechanism for the formation of ZnO/Ag heteronanostructures.

The possible mechanism for the formation of ZnO/Ag heteronanostructures is described in Scheme 1. In the first step, silver acetate decomposes to produce silver ions and acetate ions at 220 °C. At elevated temperatures, the thermal energy is sufficient to drive the silver ions (Ag^+) to the surface of the ZnO nanorods. In the second step, the acetate ions transfer electrons to the silver ions with the formation of silver nanoparticles on the surface of ZnO nanorods with the release of CO_2 and H_2.[55] The reducing environment (H_2) leads to more decomposition of silver acetate. To understand the silver deposition on the surface of ZnO nanorods better, thermal decomposition reactions were carried out at different temperatures (180 °C, 200 °C and 220 °C) and timings (30 min, 60 min and 90 min) and the ZnO/Ag samples were analyzed using FE-SEM (Figure 9).

At 220 °C, uniform deposition of silver nanoparticles on ZnO nanorods is noticed as compared to the reaction carried out at 180 °C (Figure 9a). The ZnO/Ag sample prepared at 180 °C shows adherence of a few silver nanoparticles on the surface of ZnO nanorods. The ZnO/Ag sample prepared at 200 °C shows the deposition of silver nanoparticles on ZnO nanorods but some of the ZnO nanorods are uncoated and free silver nanoparticles are also observed. The thermal decomposition carried out at 220 °C leads to good adherence of silver nanoparticles on the surface of ZnO nanorods and the SEM image does not show any free silver nanoparticles. The better deposition of silver nanoparticles on the ZnO at 220 °C

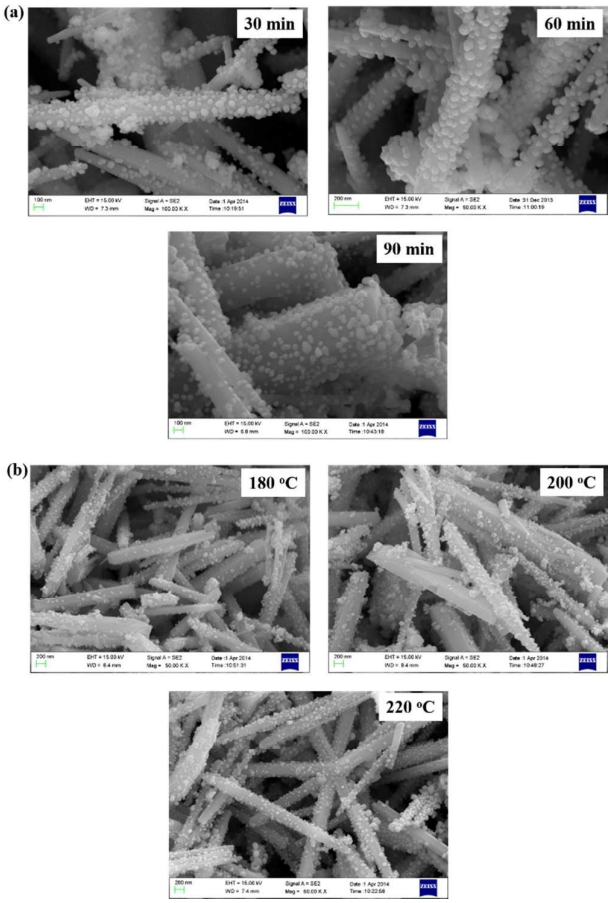

is attributed to higher rate of reduction of silver acetate at elevated temperatures.[56,57]

Fig. 9 (a) FE-SEM images of ZnO/Ag samples prepared at different thermal decomposition temperatures, and (b) FE-SEM images of ZnO/Ag samples prepared at different thermal decomposition time.

The quality of silver coating on the ZnO nanorods was also studied by varying the thermal decomposition time (at 220 °C) from 30 min to 90 min and the SEM results are shown in Figure 9b. In the case of 30 min, the average particle size of silver nanoparticles present on ZnO is 66.2 ± 17.3 nm. When the reaction time is increased to 60 min, the average particle size

of silver nanoparticles decreases to 53.5 ± 15.7 nm. When the thermal decomposition time is further increased to 90 min, an increase in the average particle size of silver (83.3 ± 19.2 nm) is observed. At lower thermal decomposition time, i.e. 30 min, only less amount of silver nuclei nucleates from the solution and during the growth stage, these fewer nuclei grow rapidly as the concentration of silver ions per silver nuclei in the solution is high and this results in an increase in the average particle size of silver.[56,57] At 60 min, nucleation takes place rapidly compared to that at 30 min thereby resulting in a decrease in the concentration of silver in the solution. This leads to decrease in the particle size of silver at 60 min as compared to that at 30 min. When the thermal decomposition time is increased to 90 min, further growth of silver nuclei occurs resulting in an increase in the average particle size of silver nanoparticles. These results conclude that the thermal decomposition time of 60 minutes and temperature of 220 °C leads to uniform deposition of silver nanoparticles on the surface of ZnO nanorods.

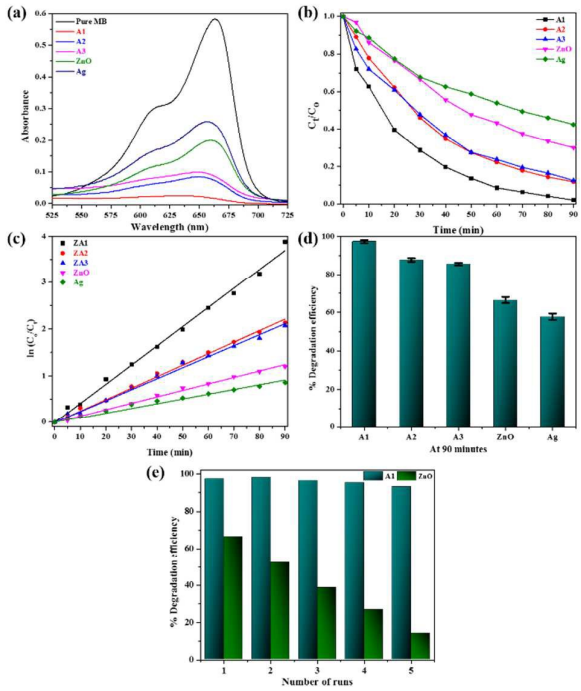

Fig. 10 (a) Photodegradation of methylene blue using ZnO nanorods, silver nanoparticles, and ZnO/Ag heteronanostructures (A1, A2, and A3), (b) comparison of photocatalytic activity of ZnO/Ag heteronanostructures (A1, A2, and A3) with ZnO nanorods and silver nanoparticles, (c) plots between $\ln(C_o/C_t)$ versus irradiation time using different photocatalysts, (d) comparison of methylene blue degradation efficiency using ZnO nanorods, silver nanoparticles and ZnO/Ag heteronanostructures (A1, A2, and A3), and (e) the recyclability (photostability) of the ZnO/Ag heteronanostructures (sample A1) and ZnO nanorods for the photodegradation of methylene blue.

4. Photocatalytic studies

The photocatalytic activity of the ZnO/Ag heteronanostructures was explored towards the photodegradation of methylene blue in an aqueous solution under sunlight and the results are shown in Figure 10. The results indicate that ZnO/Ag heteronanostructures possess higher photodegradation efficiency as compared to pristine ZnO nanorods and pure silver nanoparticles. Photodegradation of methylene blue in the absence of any catalyst under sunlight was also tested and the results indicated only a minor degradation of methylene blue. The deposition of silver nanoparticles on the ZnO nanorods enhances the degradation of methylene blue. The photodegradation of methylene blue follows pseudo-first-order kinetics which can be written as

$$\ln C_o/C_t = kt$$

where C_o and C_t are the concentrations of methylene blue at time = 0 and time = t, respectively and k is the apparent pseudo-first-order rate constant. The degradation of methylene blue by the ZnO/Ag heteronanostructures follows pseudo-first-order kinetics as indicated by a linear relationship between $ln(C_o/C_t)$ and irradiation time. The apparent pseudo-first-order rate constant (k) was calculated from the slope of the plot between $ln(C_o/C_t)$ versus time 't'. The estimated apparent pseudo-first-order rate constant (k) values for the degradation of methylene blue are 0.041, 0.025, 0.024, 0.014, and 0.010 min^{-1} for the ZnO/Ag samples A1, A2, A3, pure ZnO nanorods and silver nanoparticles, respectively. The order of degradation efficiency of photocatalysts is A1 > A2 > A3 > ZnO > Ag. The higher degradation efficiency of ZnO/Ag heteronanostructures as compared to pristine ZnO and silver nanoparticles is due to the fact that the silver nanoparticles present on the surface of ZnO nanorods act as electron sink and provides the sites for the accumulation of photogenerated electrons with an efficient charge separation of photogenerated electrons and holes.

Li et al. have evaluated the photocatalytic activity of the ZnO/Ag samples using 12 mg of the catalyst in 40 mL of the methylene blue (10 ppm) aqueous solution, under visible light for 150 minutes with the first order rate constant (k) of 1.02×10^{-2} min^{-1}.[34] Ren et al. have investigated the photocatalytic activity of ZnO/Ag films (1 cm × 2 cm) placed in 15 mL of methylene blue (2 mg/L) aqueous solution, irradiated in presence of UV light for about 90 minutes[35] and they found that the first order rate constant (k) was about 7.63×10^{-3} min^{-1}. Sun et al. have examined the photocatalytic activity of ZnO/Ag samples using 50 mL of the methylene blue (20 mg/L) aqueous solution and 50 mg of the sample.[47] The aqueous solution was irradiated in the presence of UV light and they have reported that complete degradation of methylene blue takes place in 2 h. Saravanan et al. have studied the photocatalytic activity of ZnO/Ag samples using 500 mL of 3×10^{-5} M methylene blue aqueous solution.[58] The solution was irradiated under visible light for 2 h and they have reported a first order rate constant (k) value of 3.66×10^{-4} min^{-1}. In the present study, 25 mg of

ZnO/Ag sample was dispersed in 100 mL of the 1×10^{-5} M methylene blue aqueous solution and the solution was irradiated under sunlight for about 90 minutes and the first order rate constant (k) is 4.10×10^{-2} min^{-1}. The synthesized ZnO/Ag heteronanostructures show higher rate constant (k) for the degradation of methylene blue as compared to the previous reports.

The proposed mechanism for the photodegradation of methylene blue by ZnO/Ag is shown in Scheme 2.[28,29] On illumination with sunlight, electrons (e^-) present in the valence band of ZnO are excited to the conduction band of ZnO which leaves the same amount of photogenerated holes (h^+) in the valence band. The energy of bottom of the conduction band of ZnO is higher than the Fermi energy of the ZnO/Ag heteronanostructures and the electrons in the conduction band of ZnO transfer to the silver nanoparticles. Silver acts as an electron sink which promotes interfacial charge-transfer and reduces the recombination of photogenerated electron-hole pairs. The electrons present on the surface of silver nanoparticles are trapped by dissolved oxygen (O_2) in the aqueous solution and produce superoxide radical anions ($O_2^{\bullet-}$). The photogenerated holes in the valence band of ZnO are easily trapped by H_2O and $OH^-$and hydroxyl radicals ($OH\cdot$) are produced. The active species such as holes (h^+), superoxide radical anions ($O_2^{\bullet-}$), and hydroxyl radicals ($^{\bullet}$OH) are responsible for the mineralization of methylene blue.[28,29,44] Pure Ag nanoparticles show considerable photocatalytic activity for the degradation of methylene blue and the suggested mechanism for the ability of naked silver nanoparticles in the photocatalytic degradation is as follows. On illumination with sun light, silver strongly absorbs the incident light through surface plasmon resonance (SPR) and the 5*sp* band electrons are excited to higher intraband energy levels.[59] The excited methylene blue dye molecules (MB*) inject their electrons to the 5*sp* band of silver nanoparticles via photosensitization. This reduces the concentration of holes in the 5*sp* band with reduction of recombination of excitons.[60] The electrons in the higher intraband energy levels are

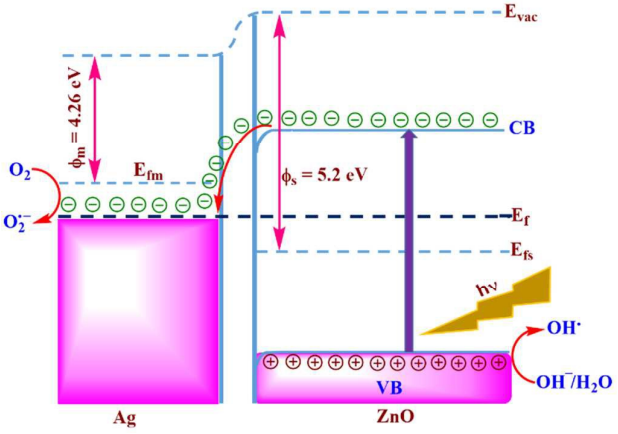

captured by oxygen with the formation of O_2^- species on the surface of silver nanoparticles. The produced O_2^- species react with H^+ and produce further reactive species such as $HO_2^{\bullet}$ and $OH^{\bullet}$ which start the degradation of methylene blue molecules.[60] The recombination rate of excitons is reduced by photosensitization which is responsible for the ability of naked Ag nanoparticles in the photocatalytic degradation of methylene blue.

Scheme 2. Proposed band structure and photocatalytic mechanism for the ZnO/Ag heteronanostructures.[28,29]

$$ZnO + h\nu \rightarrow ZnO\ (e_{CB}^- + h_{VB}^+)$$
$$Ag \rightarrow Ag^+ + e^-$$
$$e^- + O_2 \rightarrow O_2^{\bullet-}$$
$$O_2^{\bullet-} + H^+ \rightarrow HO_2^{\bullet}$$
$$HO_2^{\bullet} + HO_2^{\bullet} \rightarrow H_2O_2 + O_2$$
$$H_2O_2 + e^- \rightarrow OH^{\bullet} + OH^-$$
$$OH^{\bullet} + MB \rightarrow CO_2 + H_2O + SO_4^{2-} + NO_3^- + Cl^-$$

The enhanced photocatalytic activity of the ZnO/Ag heteronanostructures as compared to pristine ZnO nanorods and silver nanoparticles can be explained based on the photoluminescence results (Figure 8). The relationship between the photoluminescence properties and photocatalytic activity is of particular importance.[28,35] The observed photoluminescence intensity of the ZnO/Ag heteronanostructures is lower as compared to that of pristine ZnO nanorods. This indicates that the deposited silver nanoparticles on the ZnO nanorods reduce the recombination of electron-hole pairs on the surface of ZnO nanorods. Samples A2 and A3 possess larger silver nanoparticles as compared to sample A1. On illumination with sunlight, in these samples (A2 and A3), more accumulation of electrons on the silver nanoparticles happens as compared to sample A1. The photogenerated holes in valence band of the ZnO are attracted

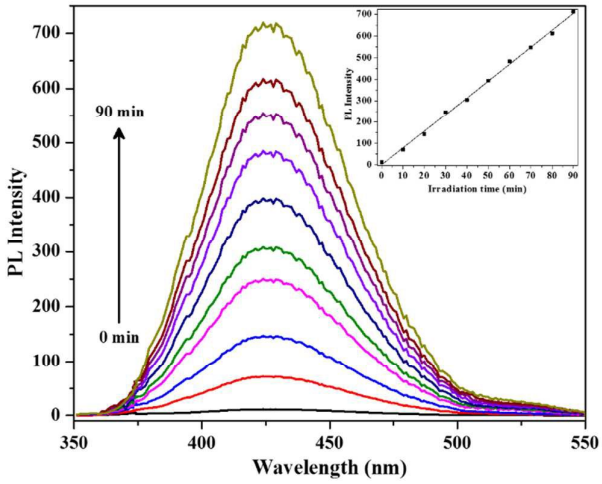

to the electrons present in silver which enhances the recombination leading to lower catalytic activity in samples A2 and A3. Also, the larger silver nanoparticles present on A2 and A3 reduces the available surface on the ZnO for light absorption thus lowering its photocatalytic activity. Sample A1 has the optimum amount /size of the silver nanoparticles on the ZnO nanorods as compared to samples A2 and A3 which

leads to an effective separation of the photogenerated electron-hole pairs.

Fig. 11 Determination of hydroxyl radicals on the surface of ZnO/Ag sample (A1) under sunlight irradiation using photoluminescence spectroscopy (λ_{exc} = 315 nm). Inset shows the plot of PL intensity versus irradiation time.

To prove the production of hydroxyl radicals on the surface of ZnO/Ag (A1) under sun light illumination, terephthalic acid (TA) was chosen as the probe molecule.[61] In a typical experiment, about 20 mg of the ZnO/Ag sample was dispersed in 50 mL of 5×10^{-4} M terephthalic acid (TA) aqueous solution containing NaOH (2×10^{-3} M). The contents were exposed to sun light for about 90 min. During the experiment, aliquots (5 mL each) were withdrawn and the solid catalyst was removed by centrifuging. The supernant solution was analyzed using PL spectroscopy (λ_{exc} = 315 nm) at regular time intervals. On sun light irradiation, the produced hydroxyl radicals readily react with terephthalic acid and produce highly fluorescent 2-hydroxy terephthalic acid (TAOH), which exhibits an emission band at about 425 nm. A gradual increase in the PL intensity at 425 nm along with irradiation time is observed (Fig. 11). The linear increase in the PL intensity with irradiation time indicates that the amount of hydroxyl radicals formed on the surface of ZnO/Ag is directly proportional to the irradiation time.

The reusability of a photocatalyst explains the stability and activity of the catalyst. One of the problems associated with ZnO as a photocatalyst is its lower photostability and it easily undergoes photoinduced dissolution.[47] The photocorrosion can be expressed as follows:

$$\mathrm{ZnO} + 2h^{+} \rightarrow Zn^{2+} + 1/2\, O_2$$

Holes in the valence band of ZnO migrate to the solid interface and react with the surface oxygen leading to the photocorrosin of ZnO. To test the photocatalytic stability (reusability) of the ZnO/Ag heteronanostructures, sample A1 (the best among the ZnO/Ag samples) was chosen and photocatalytic experiments were carried out up to 5 cycles (Figure 10e). The efficiency of the sample A1 is reduced only by 3 % after five cycles indicating good stability and durability of the ZnO/Ag heteronanostructures. On the other hand, the photostability of pristine ZnO nanorods drastically decreases due to photocorrosion. These results demonstrate the role of silver nanoparticles present on the ZnO nanorods in improving photostability of the ZnO/Ag heteronanostructures as compared to pristine ZnO nanorods.

5. Conclusions

ZnO/Ag heteronanostructures with enhanced photocatalytic activity towards the photodegradation of methylene blue in aqueous solution have been successfully synthesized through a cost effective, facile and simple thermal decomposition approach. The deposition of silver nanoparticles on the surface of ZnO nanorods greatly enhances the photocatalytic activity due to an efficient charge separation of photoinduced electron-hole pairs through Schottky barrier between the metal and semiconductor interface. The photocatalytic activity of the ZnO/Ag heteronanostructures depends on the silver loading on the ZnO nanorods. ZnO/Ag heteronanostructures with less amount of silver on ZnO nanorods provides high photocatalytic activity due to an efficient charge separation of photogenerated electron-hole pairs. The reported synthetic method can be extended to prepare other metal-semiconductor heteronanostructured materials for various functional applications.

Acknowledgements

Syam Kandula thanks the Ministry of Human Resources and Development (MHRD), Govt. of India for the financial support. The authors are thankful to the Institute Instrumentation Centre, IIT Roorkee for providing the facilities. Thanks are also due to Dr. P. A. Joy, Materials Chemistry Division, National Chemical Laboratory, Pune for his help with the XPS measurements.

Notes and references

1 A. Mclaren, T. Valdes-solis, G. Li and S. C. Tsang, *J. Am. Chem. Soc.*, 2009, **131**, 12540–12541.

2 L. Zhang, L. Tian, T. Tan, Y. Liu, D. Liu and C. Wang, *J. Mater. Chem. A*, 2015, **3**, 15265–15273.

3 A. Kar, S. Sain, S. Kundu, A. Bhattacharyya, S. Kumar Pradhan and A. Patra, *ChemPhysChem*, 2015, **16**, 1017–1025.

4 S. Huang, Y. Lin, J. Yang, X. Li, J. Zhang, J. Yu, H. Shi, W. Wang and Y. Yu, *RSC Adv.*, 2013, **3**, 20782–20792.

5 M. M. Khin, S. Nair, V. J. Babu, R. Murugan and S. Ramakrishna, *Energy Environ. Sci.*, 2012, **5**, 8075–8109.

6 Y. Wang, Q. Wang, X. Zhan, F. Wang, M. Safdar and J. He, *Nanoscale*, 2013, **5**, 8326–8339.

7 H. Wang, L. Zhang, Z. Chen, J. Hu, S. Li, Z. Wang, J. Liu and X. Wang, *Chem. Soc. Rev.*, 2014, **43**, 5234–5244.

8 R. Li, F. Zhang, D. Wang, J. Yang, M. Li, J. Zhu, X. Zhou, H. Han and C. Li, *Nat. Commun.*, 2013, **4**, 1432/1–7.

9 P. Madhusudan, J. Zhang and J. Yu, *Phys. Chem. Chem. Phys.*, 2015, **17**, 15339–15347.

10 J. Li and N. Wu, *Catal. Sci. Technol.*, 2015, **5**, 1360–1384.

11 L. Liu, W. Yang, W. Sun, Q. Li and J. K. Shang, *ACS Appl. Mater. Interfaces*, 2015, **7**, 1465–1476.

12 S. K. Dutta, S. K. Mehetor and N. Pradhan, *J. Phys. Chem. Lett.*, 2015, **6**, 936–944.

13 A. Ghosh, P. Guha, A. K. Samantara, B. K. Jena, R. Bar, S. Ray and P. V. Satyam, *ACS Appl. Mater. Interfaces*, 2015, **7**, 9486–9496.

14 M. R. Khan, T. W. Chuan, A. Yousuf, M. N. K. Chowdhury and

C. K. Cheng, *Catal. Sci. Technol.*, 2015, **5**, 2522–2531.
15 S. T. Kochuveedu, Y. H. Jang and D. H. Kim, *Chem. Soc. Rev.*, 2013, **42**, 8467–8493.
16 J. Y. Park, S. M. Kim, H. Lee and B. Naik, *Catal. Letters*, 2014, **144**, 1996–2004.
17 A. B. Djurišić, X. Chen, Y. H. Leung and A. M. C. Ng, *J. Mater. Chem.*, 2012, **22**, 6526–6535.
18 A. A. Khodja, T. Sehili, J.-F. Pilichowski and P. Boule, *J. Photochem. Photobiol. A Chem.*, 2001, **141**, 231–239.
19 C. A. K. Gouvea, F. Wypych, S. G. Moraes, N. Duran, N. Nagata and P. Peralta-Zamora, *Chemosphere*, 2000, **40**, 433–440.
20 N. Daneshvar, D. Salari and A. R. Khataee, *J. Photochem. Photobiol. A Chem.*, 2004, **162**, 317–322.
21 H. M. Chen, C. K. Chen, R.-S. Liu, L. Zhang, J. Zhang and D. P. Wilkinson, *Chem. Soc. Rev.*, 2012, **41**, 5654–5671.
22 F. Yan, Y. Wang, J. Zhang, Z. Lin, J. Zheng and F. Huang, *ChemSusChem*, 2014, **7**, 101–104.
23 L. Zhou, X. Yu and J. Zhu, *Nano Lett.*, 2014, **14**, 1093–1098.
24 N. Zhou, L. Polavarapu, Q. Wang and Q.-H. Xu, *ACS Appl. Mater. Interfaces*, 2015, **7**, 4844–4850.
25 Y. Lu, G. L. Liu and L. P. Lee, *Nano Lett.*, 2005, **5**, 5–9.
26 G. Merga, L. C. Cass, D. M. Chipman and D. Meisel, *J. Am. Chem. Soc.*, 2008, **130**, 7067–7076.
27 A. E. Kandjani, Y. M. Sabri, M. Mohammad-Taheri, V. Bansal and S. K. Bhargava, *Environ. Sci. Technol.*, 2015, **49**, 1578–1584.
28 W. Lu, S. Gao and J. Wang, *J. Phys. Chem. C*, 2008, **112**, 16792–16800.
29 Y. Zheng, L. Zheng, Y. Zhan, X. Lin, Q. Zheng and K. Wei, *Inorg. Chem.*, 2007, **46**, 6980–6986.
30 S. S. Satter, M. Hoque, M. M. Rahman, M. Y. A. Mollah and M. Abu Bin Hasan Susan, *RSC Adv.*, 2014, **4**, 20612–20615.
31 X. H. Guo, J. Q. Ma and H. G. Ge, *J. Phys. Chem. Solids*, 2013, **74**, 784–788.
32 T. Ivanova, A. Harizanova, T. Koutzarova and B. Vertruyen, *Superlattices Microstruct.*, 2014, **70**, 1–6.
33 X. Hou, *Mater. Lett.*, 2015, **139**, 201–204.
34 J. Li, J. Yan, C. Liu, L. Dong, H. Lv, W. Sun and S. Xing, *CrystEngComm*, 2014, **16**, 10943–10948.
35 C. Ren, B. Yang, M. Wu, J. Xu, Z. Fu, Y. Lv, T. Guo, Y. Zhao and C. Zhu, *J. Hazard. Mater.*, 2010, **182**, 123–129.
36 F. Li, X. Liu, Q. Qin, J. Wu, Z. Li and X. Huang, *Cryst. Res. Technol.*, 2009, **44**, 1249–1254.
37 Y. Wei, L. Ke, J. Kong, H. Liu, Z. Jiao, X. Lu, H. Du and X. W. Sun, *Nanotechnology*, 2012, **23**, 235401/1–8.
38 R. Zamiri, A. Zakaria, R. Jorfi, G. Zamiri, M. Shokati Mojdehi, H. Abbastabar Ahangar and A. Khorsand Zak, *Appl. Phys. A Mater. Sci. Process.*, 2013, **111**, 487–493.
39 C. Chen, Y. Zheng, Y. Zhan, X. Lin, Q. Zheng and K. Wei, *Dalton Trans.*, 2011, **40**, 9566–9570.
40 S. Bhattacharyya and A. Gedanken, *J. Phys. Chem. C*, 2008, **112**, 659–665.
41 W. Lu, G. Liu, S. Gao, S. Xing and J. Wang, *Nanotechnology*, 2008, **19**, 445711/1–10.
42 Q. Xiang, G. Meng, Y. Zhang, J. Xu, P. Xu, Q. Pan and W. Yu, *Sens. Actuators, B*, 2010, **143**, 635–640.
43 S. S. Warule, N. S. Chaudhari, R. T. Khare, J. D. Ambekar, B. B. Kale and M. A. More, *CrystEngComm*, 2013, **15**, 7475–7483.
44 Z. Wu, C. Xu, Y. Wu, H. Yu, Y. Tao, H. Wan and F. Gao, *CrystEngComm*, 2013, **15**, 5994–6002.
45 G. Shan, S. Zheng, S. Chen, Y. Chen and Y. Liu, *Colloids Surf., B*, 2012, **94**, 157–162.
46 S.-L. Lin, K.-C. Hsu, C.-H. Hsu and D.-H. Chen, *Nanoscale Res. Lett.*, 2013, **8**, 325/1–9.
47 F. Sun, F. Tan, W. Wang, X. Qiao and X. Qiu, *Mater. Res. Bull.*, 2012, **47**, 3357–3361.
48 S. Kandula and P. Jeevanandam, *J. Nanoparticle Res.*, 2014, **16**, 2452/1–18.
49 M. Bitenc and Z. Crnjak Orel, *Mater. Res. Bull.*, 2009, **44**, 381–387.
50 T. V Ramachandra, R. Jain and G. Krishnadas, *Renew. Sustain. Energy Rev.*, 2011, **15**, 3178–3186.
51 K. Zhong, J. Xia, H. H. Li, C. L. Liang, P. Liu and Y. X. Tong, *J. Phys. Chem. C*, 2009, **113**, 15514–15523.
52 V. Ischenko, S. Polarz, D. Grote, V. Stavarache, K. Fink and M. Driess, *Adv. Funct. Mater.*, 2005, **15**, 1945–1954.
53 H. S. Desarkar, P. Kumbhakar and A. K. Mitra, *J. Lumin.*, 2013, **134**, 1–7.
54 O. A. Yeshchenko, I. M. Dmitruk, A. A. Alexeenko, M. Y. Losytskyy, A. V. Kotko and A. O. Pinchuk, *Phys. Rev. B - Condens. Matter Mater. Phys.*, 2009, **79**, 235438/1–8.
55 P. K. Sahoo, S. S. K. Kamal, B. Shankar, B. Sreedhar and L. Durai, *J. Exp. Nanosci.*, 2012, **7**, 520–528.
56 C. Nidhi Andhariya, O. Pandey and B. Chudasama, *RSC Adv.*, 2013, **3**, 1127–1136.
57 Y. Sun, *Chem. Soc. Rev.*, 2013, **42**, 2497–2511.
58 R. Saravanan, M. Mansoob Khan, V. K. Gupta, E. Mosquera, F. Gracia, V. Narayanan and A. Stephen, *J. Colloid Interface Sci.*, 2015, **452**, 126–133.
59 C. Voisin, N. Del Fatti, D. Christofilos and F. Vallee, *J. Phys. Chem. B*, 2001, **105**, 2264–2280.
60 X. Chen, Z. Zheng, X. Ke, E. Jaatinen, T. Xie, D. Wang, C. Guo, J. Zhao and H. Zhu, *Green Chem.*, 2010, **12**, 414–419.
61 S. Liu, C. Li, J. Yu and Q. Xiang, *CrystEngComm*, 2011, **13**, 2533–2541.